Tuijin Jishu/Journal of Propulsion Technology
ISSN: 1001-4055
Vol. 46 No. 02 (2025)

Evaluation of Flow Stress in turning operation for hybrid Aluminum 6061 Composite Using Zerilli-Armstrong Model

Nandeesha Hosanagara Lokesha [1,3]*, Rajaneesh Ninganagouda Marigoudar, Deepak Swamy , Sangamesh B

[1] *Research scholar, Jain Institute of Technology, Visvesvaraya Technological University, Belagavi, India*

[2]*Professor, Department of Mechanical Engineering, Jain Institute of Technology Davanagere,Visvesvaraya Technological University, Belagavi, India*

[3]*Assistant professor, Department of Mechanical Engineering, M S Ramaih Institute of Technology Bengaluru, Visvesvaraya Technological University, Belagavi, India*

[4]*Associate Professor, School of Engineering, JNU Delhi, India*

* *Corresponding author. E-mail: hl.nandeesha@gmail.com*

Abstract

Aluminium-based composites are becoming more widely used in the aerospace, automotive and defence industries due to the demand for materials that are lightweight and high in strength, along with a continuous drive for the increase in performance. This study examined the flow stress behaviour and machinability of the Al6061 composites reinforced with yttrium oxide (Y_2O_3) and graphite particles. In total, four different combinations of Y_2O_3 were fabricated and machined as part of the controlled turning operations. Emphasis was placed on mapping the relationship between cutting forces, strain hardening and thermal softening whilst machining. The Zerilli-Armstrong (Z-A) constitutive model incorporates the effects of dislocation mechanics and thermal activation processes in modelling flow stress behaviour. As part of the research finite element analysis (FEA) was undertaken to perform machining simulations, particularly in relation to the stress, strain and temperature distributions being generated in the cutting zone. The results in both conditions concluded that the Z-A model more accurately described the deformation response of the reinforced Al6061 composites under different machining conditions.

***Keywords**: Aluminium 6061, yttrium oxide, flow stress, Zerilli-Armstrong*

1 Introduction

Composites made of aluminium have improved mechanical properties as a result of the aerospace, automotive, and defence industries growing need for lightweight, high-strength materials [1]. To increase its strength, resistance to wear, and thermal stability, aluminium 6061 (Al6061), a common precipitation-hardened alloy, is frequently reinforced with ceramic or solid lubricant particles [2-5]. It is crucial to precisely model the flow stress behaviour of the material during machining operations because the incorporation of reinforcements like graphite and yttrium oxide (YO_3) drastically changes the material's deformation characteristics [6-8].

Knowing how these material changes impact plastic deformation, strain hardening, and dynamic strain rate sensitivity is one of the main challenges in machining aluminium composites [9-12]. The workpiece experiences intricate thermo-mechanical loading during turning operations, which affects surface integrity, tool wear, and cutting forces [13-15]. The Zerilli-Armstrong (Z-A) equation offers an alternative that explicitly takes into account the role of dislocation motion and thermal activation in FCC metals, making it ideal for materials like Al6061 composites[26-34]. Traditional empirical constitutive models, like the Johnson-Cook (J-C) model, are a popular method for modelling flow stress [35].

The Zerilli-Armstrong model is a physically based constitutive equation that accounts for strain, strain rate, and temperature effects on material behaviour [36]. Unlike the Johnson-Cook model, which primarily relies on empirical fitting parameters, the Z-A model integrates dislocation mechanics to describe plastic flow, making it more adaptable to a wide range of machining conditions [37]. For face-centered cubic (FCC) metals such as aluminium, the Z-A equation will be used to find the flow stress.

In this study, a specimen of Al6061 composite material was fabricated with Y_2O_3 and graphite as reinforcements with four combinations of yttrium oxide. Turning operations were conducted under controlled machining conditions, the primary objective is to establish a correlation between cutting forces, strain hardening, and thermal softening mechanisms during machining. Additionally, finite element analysis (FEA) was employed to validate experimental results by simulating the turning operation under similar cutting conditions. The computational analysis helps in understanding the distribution of stress, strain, and temperature gradients across the machining zone, and the flow stress of the material was evaluated using the Zerilli-Armstrong equation. Further confirming the accuracy of the Z-A model in predicting the flow stress behaviour of the reinforced Al6061 composite.

This research provides significant insights into the deformation behaviour, machinability, and mechanical response of aluminium-based composites, contributing to better predictive models for high-performance machining applications. The findings will assist in optimizing cutting parameters, tool design, and material selection for machining Al6061 composites, ultimately leading to improved productivity and component performance.

2 Methodology

2.1 Casting

Stir casting is one of the most commonly used and cost-effective methods for fabricating aluminium matrix composites (AMCs). In this process, the aluminium is first melted in a furnace and then maintained at a controlled temperature slightly above its melting point. Reinforcement particles, such as ceramics or graphite, are preheated to remove moisture and then gradually added to the molten aluminium. A mechanical stirrer is used to create a vortex in the melt, ensuring uniform distribution of the reinforcement throughout the matrix. The stirring action also helps improve the wettability between the aluminium and the reinforcement particles. After sufficient mixing, the composite slurry is poured into a preheated mould and allowed to solidify. Stir casting offers simplicity, scalability, and suitability for large-scale production. However, careful control of process parameters such as stirring speed, time, and temperature is essential to prevent clustering or sedimentation of the reinforcement and to ensure a defect-free, homogeneous microstructure.

Table 1

Property	**Al 6061**
Young's modulus	0.689 GPa
Poisson's ratio	0.33
Tensile yield stress	0.276 GPa
Ultimate tensile strength	0.310 GPa
Brinell hardness	95

The base metal Aluminum 6061 has been chosen as a matrix material and its mechanical properties has been recorded in the table 3 [1-2]. Reinforcement materials used in this experiment is yttrium oxide and graphite. The material property of these reinforcement materials are listed in the table 2 [4-8].

Table 2

Property	Values of Yttrium oxide	Values of Graphite
Tensile Strength	0.15 GPa	0.15 – 0.30Gpa
Young's Modulus	160 Gpa	10 – 20Gpa
Poisson's Ratio	0.298	0.1 – 0.3
Coefficient of Friction	0.35	0.10 – 0.20
Melting temperature	2450°C	3652°C
Particle size	100µ	100µ

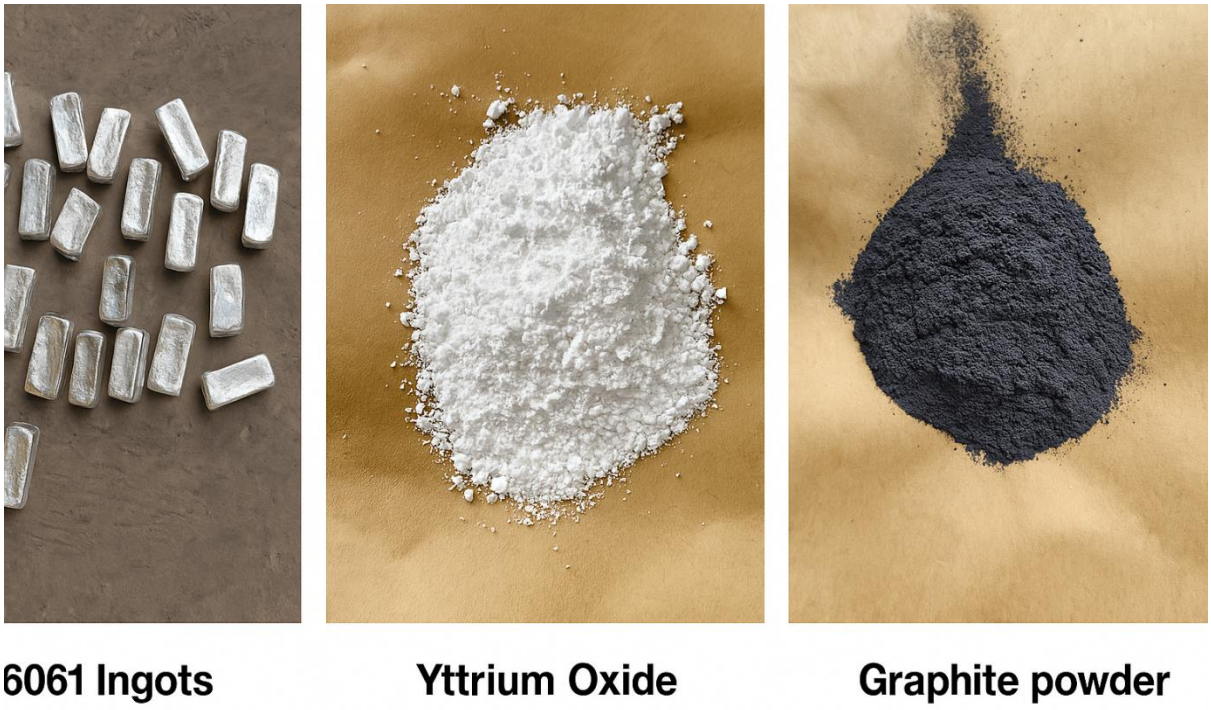

Fig 1: Base metal and reinforcements

In the above case study of stir casting technique was employed in producing a composite of aluminium 6061 alloy, Aluminium ingots were subjected to melting and maintaining the reinforcing elements distributed at equal levels throughout the molten metal. Powdered yttrium oxide as well as powder graphite were also added (shown in fig 1), maintaining graphite at the same one percent of the whole weight and another at 0.5, 1.0, 1.5, and 2.0 percent of that of yttrium oxide against the weight of aluminium. Yttrium oxide was changed, whereas stir casting process was used to attain homogenization of reinforcement within the aluminium matrix (shown in fig 2).

Fig 2: Stirr casting of hybrid composite in a furnce

Besides these four strengthened samples, one pure as-cast aluminium sample was prepared for comparative purposes. Additional tests were performed to analyse the mechanical and physical properties of aluminium hybrid composite. The systematic procedure employed in modifying the design parameters of the composites and applying stir casting ensured a well-controlled macrostructure of composites which would be useful in enhancing the material's multi-functional properties**2.2 casting validation**

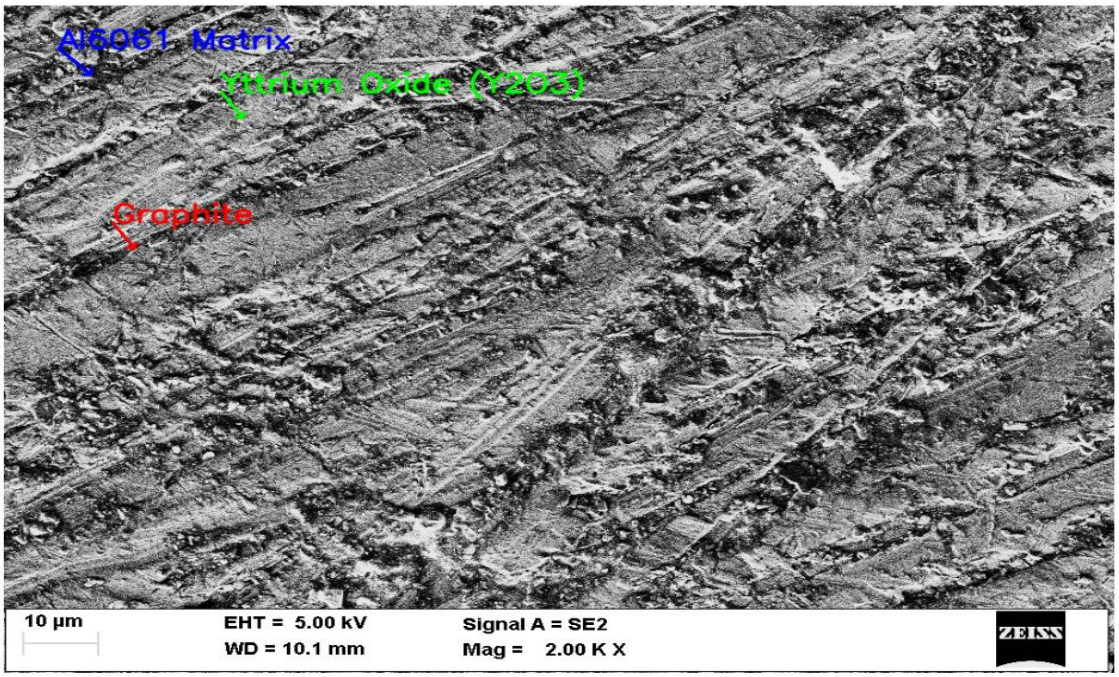

Fig 3: SEM image of hybrid composite

The microstructural analysis of an aluminium 6061 hybrid composite reinforced with graphite and yttrium oxide (Y_2O_3) is depicted in the provided SEM (Scanning Electron Microscope) image shown in fig 3. The uniform distribution of reinforcements within the Al6061 matrix is visible in the image, which was taken at a magnification

of 2000x and the specimen here shown is 1% of Yttrium oxide reinforced one. Particles of yttrium oxide are represented by the bright areas, whereas graphite is present in the darker areas. The SEM analysis enhances mechanical properties by confirming a strong bond between the reinforcements and the matrix. This composite is appropriate for structural applications because of the fine distribution of yttrium oxide, which improves hardness and wear resistance, and the addition of graphite, which improves lubricating qualities.

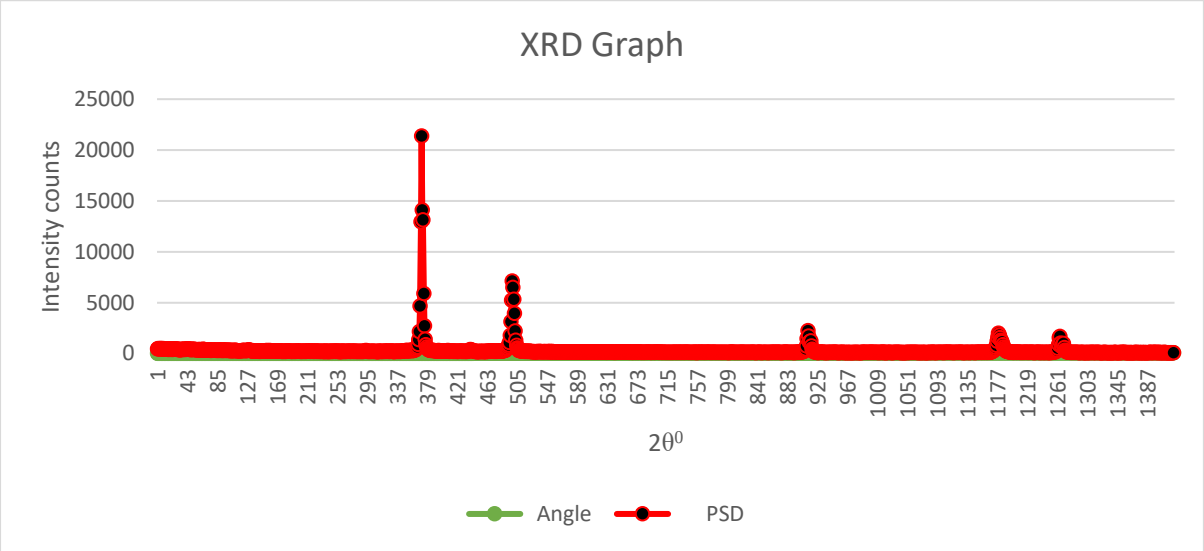

Fig 4: XRD graph of Hybrid composite.

The crystalline structure of the Al6061 composite reinforced with graphite and yttrium oxide (Y_2O_3) is depicted in the XRD (X-ray diffraction) graph above in the fig 4. The spectrum's peaks, which show the existence of several crystalline phases, attest to the reinforcements' effective integration into the aluminium matrix (for specimen 1% of Yttrium oxide reinforced one). Good crystallinity and uniform dispersion of Y_2O_3 and graphite particles are suggested by the sharp and well-defined peaks, especially in the higher intensity regions. The homogeneous distribution of reinforcements throughout the matrix is further supported by the lack of unexpected or irregular peaks. All things considered, the XRD pattern confirms the composite's structural soundness and the calibre of the stir casting.

2.3 Mechanical property testing

Fig 5: Tensometer setup for finding young’s modulus.

Tensometer is used to determine the tensile strength and other mechanical properties of materials under axial loading shown in fig 5. It assesses how a material responds when a force is applied in the direction of tension, determining important properties like yield strength, ultimate tensile strength, elongation, and Young's modulus. The test piece is held firmly on both ends and extended at a controlled speed until it fails. This tensometer is fitted with digital sensors and software for precise data acquisition and analysis. This needs smaller specimen than UTM's. Hence the material require for this instrument is less and machining time will be reduced for making it. Aluminum specimens are prepared to ASTM E8/E8M standard(Gauge Dia 6mm,Gauge length 26mm and Gripping Dia 9mm), ensuring uniform cross-sectional area and smooth surfaces to minimize stress concentrations Shown in fig 6.

Fig 6: Tensometer specimen prepared in turning operation

For experimental reasons, a lathe tool dynamometer was utilized to record cutting forces in the longitudinal, radial, and tangential directions shown in fig 7. The cutting tool utilized in this research was a CNMG 120408 MS LF6118 turning insert. Various combinations of turning parameters were performed to examine the behaviour of various specimens. Various iterations were carried out to collect precise and uniform data for every specimen. The dynamometer provided accurate measurement of cutting forces with great insight into machining performance and material behaviour. The setup proved vital in the assessment of machinability of the composite materials produced under differing conditions.

Fig 7: Lathe tool dynamometer setup.

Lathe tool dynamometer is advanced one and it has got sensors and software's for accurate

Fig 8: Lathe tool dynamometer generate graph on computer screen.

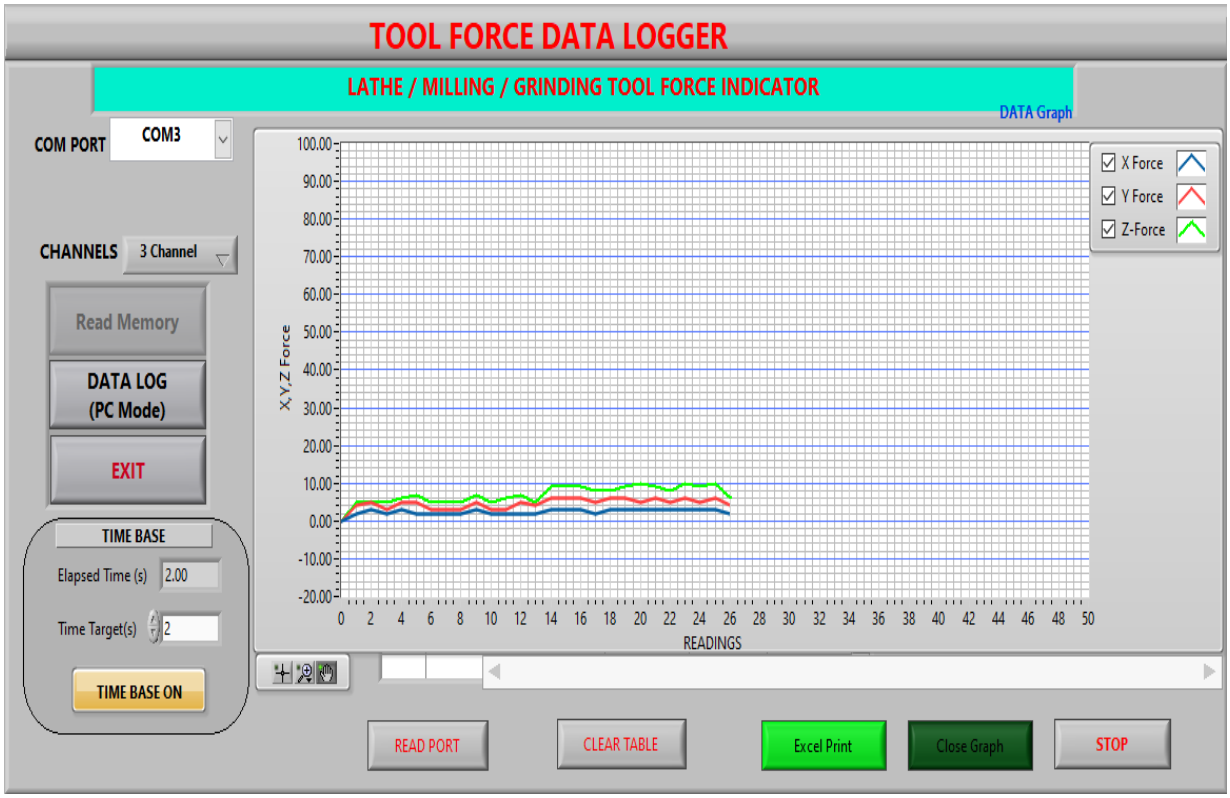

forces, here in this fig 8 shows the cutting graph generated by the software of dynamometer in 3 different colored lines which tells us the cutting force ratios. This graph is redrawn and explained in result and discussion.

3. Result and discussion

3.1 Cutting force calculations

In this experiment, turning forces were measured using three key variables: cutting speed, feed rate, and depth of cut. The lathe tool dynamometer setup was initiated by resetting the sensor and starting the data logging software.

Table 3

Levels	**Parameter**	**Itirations**			
		1	**2**	**3**	**4**
A	Cutting speed (m/min)	23.56	39.58	67.86	113.1
B	Feed rate (mm/rev)	0.05	0.1	0.15	0.2
C	Depth of cut (mm)	0.2	0.3	0.4	0.5

The cutting speed and feed were held constant at 23.56 m/min and 0.05 mm/rev, respectively, while the depth of cut was varied from 0.2 mm to 0.5 mm, as listed in Table 3. Forces were recorded from the most frequently occurring values in the log, representing the typical resistance the tool experiences during operation. A total of 256 turning force readings were obtained by varying two parameters while keeping one constant in each set, with 64 combinations tested. The results showed that cutting force (Fz) was the highest, followed by thrust force (Fy)

and feed force (Fx). An incremental 2–3% rise in cutting force was observed with each iteration due to increased depth of cut.

During the second group of machining trials, the depth of cut (0.5 mm) and cutting speed (39.58 m/min) were kept as constants, but feed rate varied from 0.05 to 0.2 mm/rev. The dynamometer measured equal forces as the tool cut into the material. Cutting, feed, and thrust forces were taken from the most prevalent values within the data log and reflect the normal operating loads experienced by the tool. The graph verifies that increasing feed rate yields greater cutting forces.

In the third trial series, feed (0.05 mm/rev) and depth of cut (0.5 mm) were fixed, with speed ranging from 23.56 m/min to 113.1 m/min. The forces were measured and calculated using the most frequent values on the log, indicating smooth force levels experienced during use.

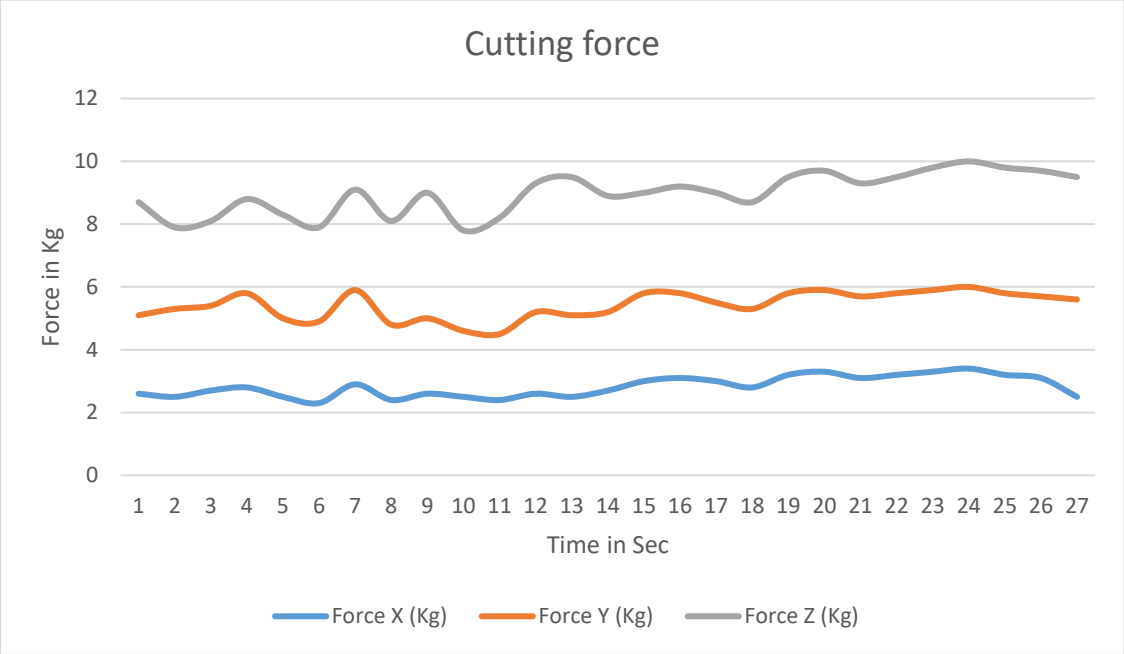

Fig 9: cutting force graph for the specimen 2 (1% Yttrium oxide & 1% Graphite)

X-Axis Force (Blue Line): This is a measure of feed force, and it is the least of the three factors. Small changes account for variations in tool-workpiece contact and feed rate. With graphite present, there is friction reduction leading to overall stability with low feed force. With yttrium oxide addition, an increase in the hardness of the composite introduces minute changes in this force as shown in fig 9.

Y-Axis Force (Red Line): Refers to the thrust or radial force and is of moderate amplitude. Fluctuations imply varying tool engagement, hardness of the composite, and wear of the tool. Yttrium oxide enhances hardness and offers enhanced cutting resistance, whereas graphite reduces adhesion on the tool surface, preventing peak force spikes. The moderate variance signifies stable cutting with periodic hard spots due to inhomogeneous reinforcement.

Z-Axis Force (Green Line): This is the predominant cutting force and the highest of the three. The plot is generally on the rise with fluctuations, which is due to strain hardening in Al6061 with progressing cutting. Yttrium oxide increases hardness further, requiring more force to remove chips. Fluctuations are due to non-uniform reinforcement and wear of the tool, while a gentle dip towards the end may suggest edge wear, which makes the cutting less aggressive.

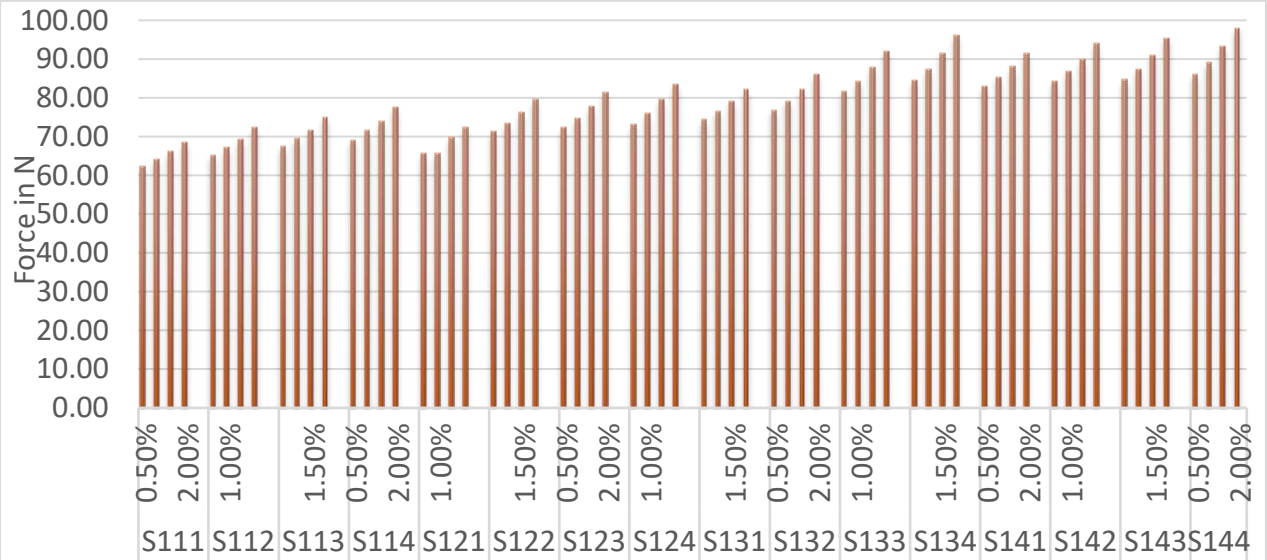

Fig 10: Bar chart for cutting force on all the specimens

The bar graph shows cutting forces measured during turning operations with different combinations of feed rate and depth of cut, and a constant cutting speed. The x-axis refers to sample identifiers and percentages of reinforcement, and the y-axis reflects the cutting force in Newtons (N). It is clear that a higher feed rate and depth of cut lead to an increase in cutting force. The samples with increased percentages of reinforcement, especially 2.00%, have greater cutting forces as a result of higher material hardness. The trend is one of uniform increase in cutting force from S111 to S144, indicative of the combined effect of machining parameters and composition of the composite.

3.2 Young's model calculations

The Tensometer graph displays a typical stress-strain curve for a composite material under tensile loading shown in fig 11. It shows an initial elastic region followed by a plastic deformation phase, indicating ductile behaviour. The curve peaks at ultimate tensile strength, after which necking and eventual fracture occur, Young's modulus of the materials has been found using the slopes of the graph.

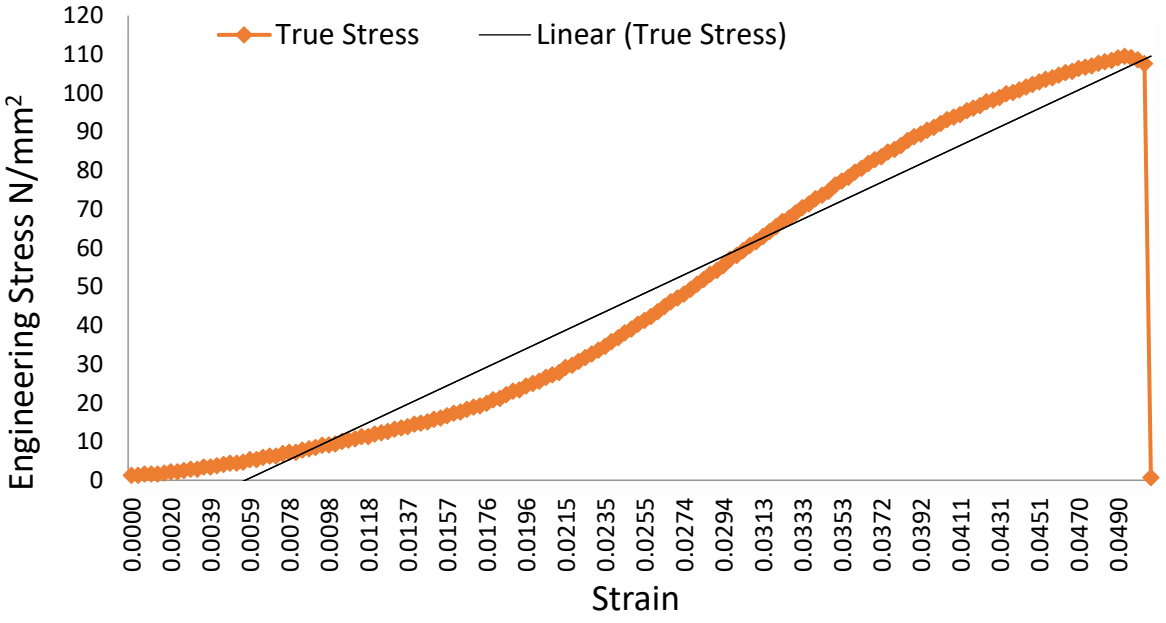

Fig 11: stress strain graph generated from tensometer result.

The slope of the line represents the change in stress divided by the change in strain:

$$E=\Delta\sigma/\Delta\epsilon \quad (1)$$

Where:

- E is Young's modulus.
- $\Delta\sigma$ is the change in stress.
- $\Delta\epsilon$ is the change in strain.

From the equation we can see that the slope (m) is 0.795. Since the graph is in terms of Eng Stress (N/mm2) and Strain:

$E=0.795/1.1$ N/mm^2

E=0.715 Gpa

This is the Young's modulus of the specimen with 1% Y_2O_3

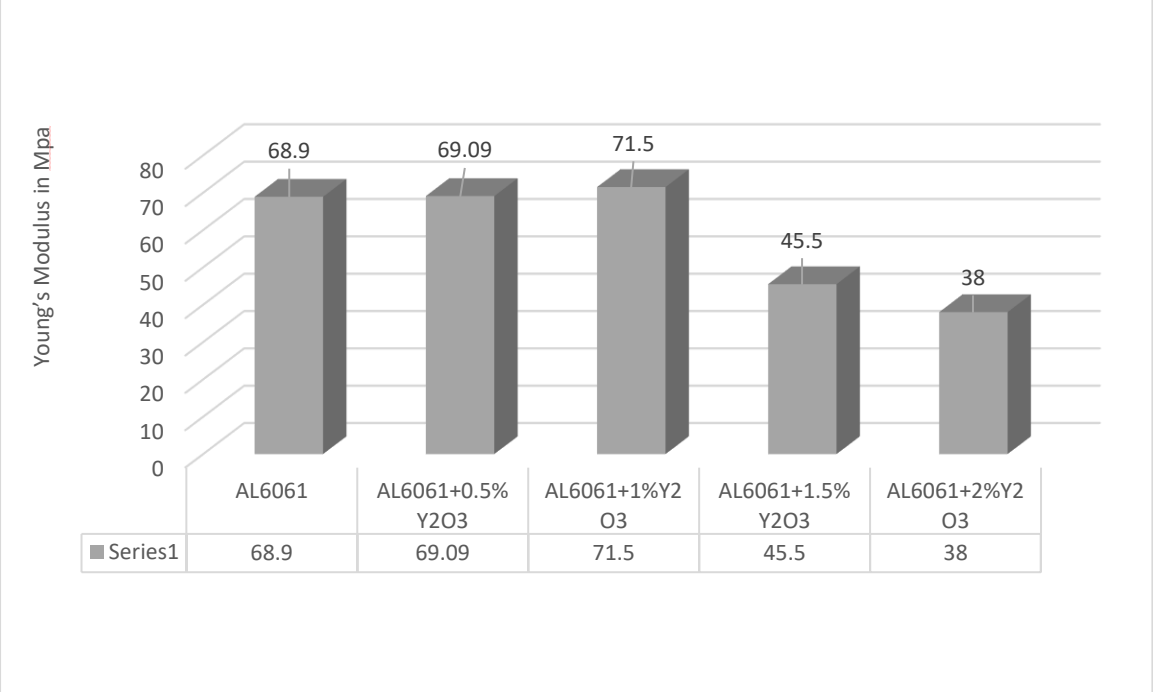

Fig 12: Young's modulus of all the specimens

The Young's modulus behaviour of various (Al6061) hybrid composites that are Yttrium oxide (Y_2O_3) sintered have been diagrammatically represented in the above obelisk. The base Al6061 has a Young's modulus 68.9 MPa (shown in fig 12). When a 0.5% Y_2O_3 is added, a small increase is noted which rises to 69.09 MPa. This likely suggests a scepticism effect of reinforcement. The maximum value of 71.5 MPa was obtained at an alloy of 1% Y_2O_3 and indicates optimum distribution of reinforcing particles and strengthening of the plastic matrix. However, this value has been decreases drastically to 45.5 at 1.5% Y_2O_3, falling further to 38 MPa, at 2% Y_2O_3. This low value suggests weak bonding between the particles, agglomeration of particles, and matrix weakening at higher Y_2O_3 concentrations. The graph demonstrates certain ration supports mechanical properties improvement. Too much Y_2O_3 structural inefficiencies composites tensile properties because of inadequate distribution and reinforcement composite material fragment brittle.

3.3 Hardness

The hardness values of Al6061 composites modified with different proportions of yttrium oxide (Y_2O_3) along with 1% constant graphite (Gr) and measured on the HRB scale are represented in the provided figure 13.

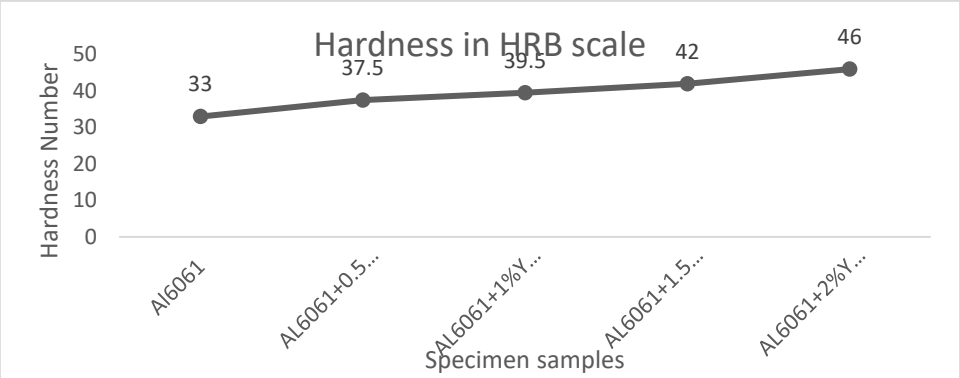

Fig 13: Result of hardness test for all the specimens

The base Al6061 shows hardness of 33 HRB. The introduction of 0.5% Y_2O_3 and 1% Gr enhances the hardness to 37.5 HRB, indicating a strengthening effect. With an increase in Y_2O_3 to 1% the hardness further increases to 39.5 HRB. This trend continues when 1.5% Y_2O_3 is added, achieving 42 HRB. The highest hardness of 46 HRB is recorded with 2% Y_2O_3, indicating significant improvement due to uniform dispersion of reinforcements. The increase in hardness is due to the incorporation of Y_2O_3, which has a hard ceramic nature, and to the lubrication effect of graphite that diminishes plastic deformation. This graphs prove that with the addition of Y_2O_3, the hardness increases and the composite becomes more durable against wear and deformation.

3.4 Cutting Force Validation

Under machining of aluminium, the surface is subjected to plastic deformation through mechanical interaction with the cutting tool. The degree of this deformation is a function of parameters like feed rate, cutting tool geometry, and general machining conditions. When yttrium oxide (Y_2O_3) particles are incorporated in the aluminium matrix, they create localized stress concentrations upon cutting as shown in fig 14. These stress concentrations are likely to be greater near the reinforcement particles than in the surrounding softer aluminium with the potential to initiate different modes of failure. One of them is interfacial debonding between aluminium and the yttrium oxide due to mechanical property mismatch leading to microcracks. Another one is excessive stress near the reinforcement particles leading to fractures either in the aluminium matrix or, in the worst-case scenario, within the yttrium oxide particles themselves. In order to learn more about such effects, Finite Element Analysis (FEA) can be employed to simulate the machining process and compute the stress distribution and thereby predict likely failure areas and enhance composite design.

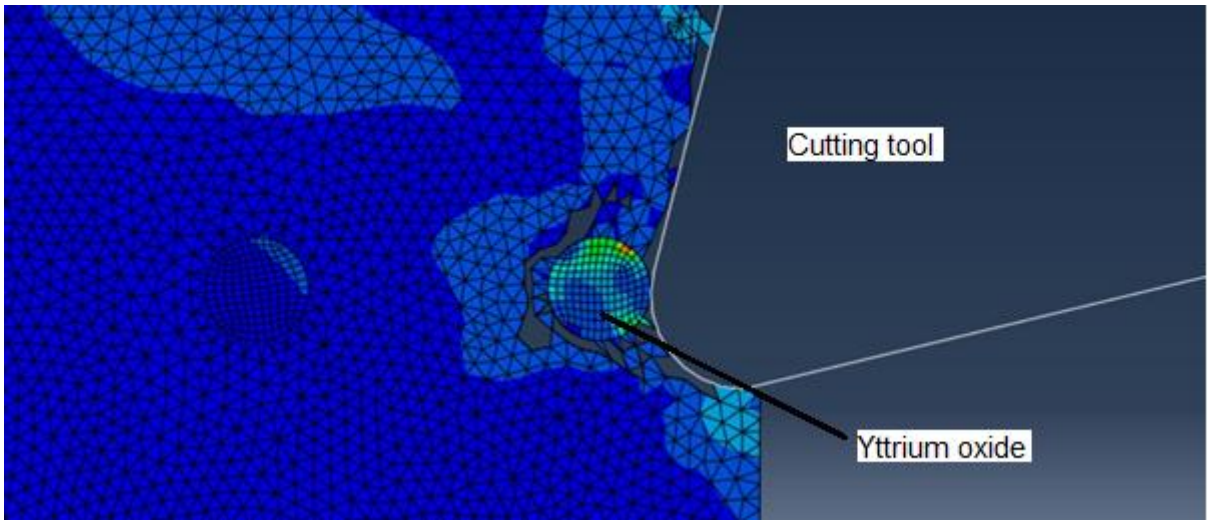

Fig 14: Virtual machining of the model by FEA method using Ansys software.

Figure 15 is an ANSYS cutting force analysis, with time (s) along the x-axis and cutting force (N) along the y-axis, for a very short period of time from 0 to 0.01 seconds. The force is initially close to zero, representing no contact. There is a sudden plunge into negative values at approximately 0.0025 seconds, which represents initial resistance upon material-tool engagement. The graph subsequently shows several peaks and troughs, possibly a result of tool vibrations, chip creation, or material irregularities. The biggest drop in force, around 66.985 N, at around 0.005 seconds could be the result of instantaneous resistance. The rapid fluctuations continue, and around 0.01 seconds, the force suddenly increases, possibly signifying the conclusion of cutting or a critical change in cutting conditions.

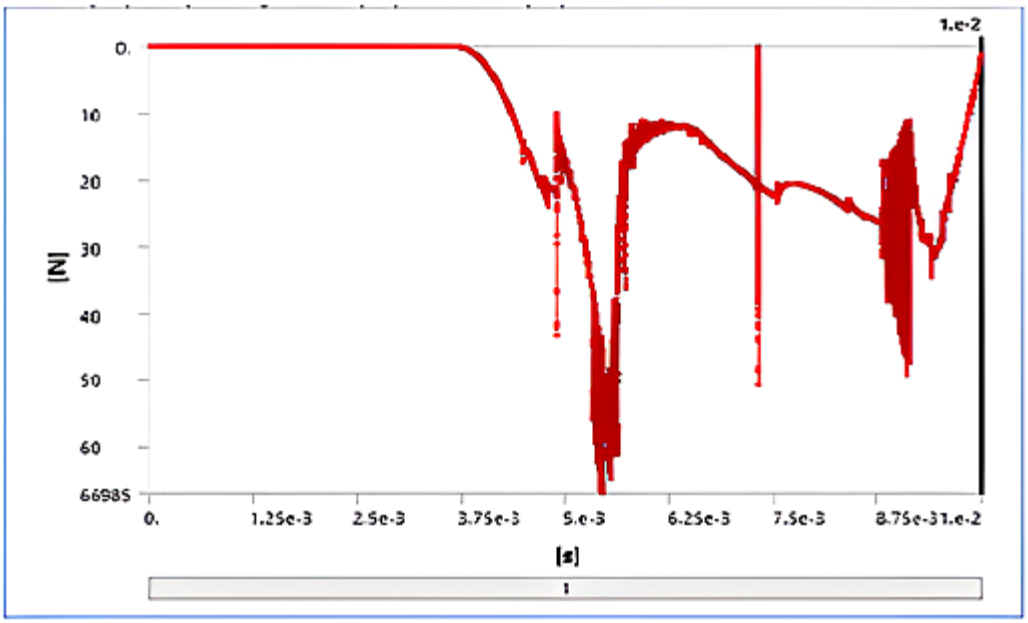

Fig : 15 Cutting force graph generated by ANSYS

3.5 Zerilli-Armstrong Equation for Flow Stress

Zerilli-Armstrong Equation for Flow Stress is as follows.

$$\sigma = \sigma_0 + B\varepsilon^n + Ce^{(-\beta T)} \ln(\dot{\varepsilon} + 1) \quad (2)$$

Where:

σ = Flow stress (MPa)

σ_0 = Initial yield stress (MPa)

B = Strain-hardening coefficient

ε = True plastic strain

n = Strain-hardening exponent

C = Strain-rate sensitivity coefficient

$\dot{\varepsilon}$ = Strain rate (s^{-1})

T = Temperature (K)

β = Thermal activation parameter

After all the calculations of Zerilli Armstrong equation, the values are recorded in the table 14.

Table 4

Si Number	Zerilli-Armstrong flow stress in MPa	Specimen composition
	370.2	Aluminium 6061
	387.45	Aluminium 6061+0.5% Y_2O_3+1%Graphite
	401.675	Aluminium 6061+1% Y_2O_3+1%Graphite
	415.95	Aluminium 6061+1.5% Y_2O_3+1%Graphite
	424.6	Aluminium 6061+2% Y_2O_3+1%Graphite

The table presents the Zerilli-Armstrong flow stress values in MPa for various compositions of Aluminium 6061 reinforced with Y_2O_3 and graphite. The base material, Aluminium 6061, exhibits a flow stress of 370.2 MPa. With the addition of 0.5% Y_2O_3 and 1% graphite, the stress increases to 387.45 MPa, indicating improved strength. A further increase in Y_2O_3 content to 1%, 1.5%, and 2%, while keeping graphite constant at 1%, results in progressive rises in flow stress to 401.675 MPa, 415.95 MPa, and 424.6 MPa, respectively. This trend suggests that Y_2O_3 reinforcement significantly enhances the material's resistance to deformation, likely due to grain refinement and increased dislocation hindrance, making these composites promising for high-strength lightweight applications.

Conclusion

This research focused on analysing the cutting forces and flow stress behaviour of Al 6061 composites reinforced with 1% Y_2O_3 and 1% graphite through a combination of experimental turning tests and finite element modelling using ANSYS. The experimental results closely aligned with the FEM simulations, validating the model's reliability in accurately predicting cutting forces.

- Composite is perfectly homogeneous and it has been verified in both XRD test as well as SEM images.
- As the hardness of each specimen increased gradually, the cutting force also increased. This indicates a consistent and expected relationship between hardness and cutting force.
- There is a correlation in between physical turning force measurement and virtual force measurement, both are matching upto 90%
- Comparatively, reinforcement of 1% of yttrium is optimum because it has good flow stress resistance and increased in Young's modulus also, afterwards Young's modulus will be gradually reduced.
- Henceforth reinforcement of yttrium oxide and graphite are increased mechanical strength as well as resistance to deformation in aluminum6061.

References

[1] G. E. Totten, D. S. MacKenzie, "Handbook of Aluminum: Vol. 1: Physical Metallurgy and Processes," CRC Press, 2003.

[2] Properties and Selection: Nonferrous Alloys and Special-Purpose Materials. ASM International, 1990. doi: 10.31399/asm.hb.v02.9781627081627.

[3] M. C. Chaturvedi, *Welding and joining of aerospace materials*. Woodhead Publishing, 2022. Accessed: Jul. 06, 2024. [Online]. Available: http://www.sciencedirect.com:5070/book/9780128191408/welding-and-joining-of-aerospace-materials

[4] J. guang Li and S. qi Wang, 'Distortion caused by residual stresses in machining aeronautical aluminum alloy parts: recent advances', *International Journal of Advanced Manufacturing Technology*, vol. 89, no. 1–4. Springer London, pp. 997–1012, Mar. 01, 2017. doi: 10.1007/s00170-016-9066-6.

[5] Sajjadi, S. A., Ezatpour, H. R., & Beygi, H. (2012). Microstructure and mechanical properties of Al–Al2O3 micro and nano composites fabricated by stir casting. *Materials Science and Engineering: A*, 528(3), 8765-8771.

[6] L. Yang, C. Xu, B. Fu, and M. Zhang, 'Simulation Research on Vibration Cutting Mechanism of Metal Matrix Composites', in *IOP Conference Series: Materials Science and Engineering*, Institute of Physics Publishing, Oct. 2019. doi: 10.1088/1757-899X/611/1/012012.

[7] M. A. Sougavabar, S. A. Niknam, and B. Davoodi, 'Experimental characterization of tool wear morphology in milling of Al520-MMC reinforced with SiC particles and additive elements Bi and Sn', *Journal of Materials Research and Technology*, vol. 24, pp. 571–585, May 2023, doi: 10.1016/j.jmrt.2023.03.006.

[8] 'National Technical Reports Library'.

[9] M. Akhtar, S. Z. Qamar, M. Muhammad, and A. Nadeem, 'Optimum heat treatment of aluminum alloy used in manufacturing of automotive piston components', *Materials and Manufacturing Processes*, vol. 33, no. 8, pp. 905–912, 2018, doi: 10.1080/10426914.2017.1398230.

[10] M. H. Idris, M. S. Salleh, and M. Z. Omar, 'The effect of heat-treatment on aluminum-based piston alloys', *Materials Science and Engineering: A*, vol. 528, no. 3, pp. 812–819, 2010, doi: 10.1016/j.msea.2010.09.074.

[11] J. guang Li and S. qi Wang, 'Distortion caused by residual stresses in machining aeronautical aluminum alloy parts: recent advances', *International Journal of Advanced Manufacturing Technology*, vol. 89, no. 1–4. Springer London, pp. 997–1012, Mar. 01, 2017. doi: 10.1007/s00170-016-9066-6.

[12] J. P. Davim, C. Maranhão, M. J. Jackson, G. Cabral, and J. Grácio, 'FEM analysis in high speed machining of aluminium alloy (Al7075-0) using polycrystalline diamond (PCD) and cemented carbide (K10) cutting tools', *International Journal of Advanced Manufacturing Technology*, vol. 39, no. 11–12, pp. 1093–1100, Dec. 2008, doi: 10.1007/s00170-007-1299-y.

[13] A. P. Zhilyaev, T. G. Langdon, 'Microstructural and mechanical characterization of aluminum alloy processed by equal channel angular pressing', Materials Science and Engineering: A, vol. 486, no. 1–2, pp. 123–129, 2008, doi: 10.1016/j.msea.2007.08.019.

[14] M. R. Ghomashchi, A. Vikhrov, 'Effect of heat treatment on microstructure and mechanical properties of 6061 aluminum alloy', Journal of Materials Processing Technology, vol. 170, no. 1–2, pp. 427–433, 2005, doi: 10.1016/j.jmatprotec.2005.06.067.

[15] S. S. Joshi, S. S. Pande, and P. K. Brahmankar, 'Modeling and optimization of cutting forces in turning of Al/SiC particulate composites', Journal of Materials Processing Technology, vol. 183, no. 2–3, pp. 251–259, 2007, doi: 10.1016/j.jmatprotec.2006.10.021.

[16] M. Nouari and G. List, 'Wear characteristics and performance of carbide tools when dry machining AlSi alloys', International Journal of Machine Tools and Manufacture, vol. 53, no. 1, pp. 68–81, 2012, doi: 10.1016/j.ijmachtools.2011.09.007.

[17] A. M. Abuelnaga, M. A. Elbestawi, and A. K. Srivastava, 'Tool wear in high-speed turning of Al-20% Si alloy', Wear, vol. 188, no. 1–2, pp. 50–56, 1995, doi: 10.1016/0043-1648(95)06660-5.

[18] M. A. Davies, T. Ueda, R. M'Saoubi, B. Mullany, and A. L. Cooke, 'On the measurement of temperature in material removal processes', CIRP Annals, vol. 56, no. 2, pp. 581–604, 2007, doi: 10.1016/j.cirp.2007.10.009.

[19] M. Nouari, G. List, F. Girot, and D. Coupard, 'Experimental analysis and optimization of tool wear in dry machining of aluminum alloys', Wear, vol. 255, no. 7–12, pp. 1359–1368, 2003, doi: 10.1016/S0043-1648(03)00262-3

[20] M. J. Roy and D. M. Maijer, 'Analysis and modeling of a rotary forming process for cast aluminum alloy A356', Journal of Materials Processing Technology, vol. 223, pp. 1–10, 2015, doi: 10.1016/j.jmatprotec.2015.03.023.

[21] K. C. Le and T. M. Tran, 'Dislocation mediated plastic flow in aluminum: Comparison between theory and experiment', International Journal of Plasticity, vol. 95, pp. 1–12, 2017, doi: 10.1016/j.ijplas.2017.04.001.

[22] M. Khajehzadeh and M. R. Razfar, 'FEM and Experimental Investigation of Cutting Force During UAT Using Multicoated Inserts', *Materials and Manufacturing Processes*, vol. 30, no. 7, pp. 858–867, Jul. 2015, doi: 10.1080/10426914.2014.973590.

[23] V. Madhavan and A. H. Adibi-Sedeh, 'Understanding of finite element analysis results under the framework of Oxley's machining model', *Machining Science and Technology*, vol. 9, no. 3, pp. 345–368, Jul. 2005, doi: 10.1080/10910340500196587.

[24] X. Teng, D. Huo, W. Chen, E. Wong, L. Zheng, and I. Shyha, 'Finite element modelling on cutting mechanism of nano Mg/SiC metal matrix composites considering cutting edge radius', *J Manuf Process*, vol. 32, pp. 116–126, Apr. 2018, doi: 10.1016/j.jmapro.2018.02.006.

[25] X. Teng, D. Huo, W. Chen, E. Wong, L. Zheng, and I. Shyha, 'Finite element modelling on cutting mechanism of nano Mg/SiC metal matrix composites considering cutting edge radius', *J Manuf Process*, vol. 32, pp. 116–126, Apr. 2018, doi: 10.1016/j.jmapro.2018.02.006.

[26] X. Teng, D. Huo, W. Chen, E. Wong, L. Zheng, and I. Shyha, 'Finite element modelling on cutting mechanism of nano Mg/SiC metal matrix composites considering cutting edge radius', *J Manuf Process*, vol. 32, pp. 116–126, Apr. 2018, doi: 10.1016/j.jmapro.2018.02.006.

[27] Zerille, J. & Armstrong, P. (1969). "A Flow Stress Equation for Deforming Polycrystals". *Transactions of the Metallurgical Society of AIME*, vol. 245, pp. 1199–1205, 1969. Armstrong, P. & Zerille, J. (1971). "The Role of Temperature in the Flow Stress Behavior of Metals". *Journal of Materials Science*, vol. 6, no. 3, pp. 424–430, 1971.

[28] Zerille, J., Armstrong, P., & Robertson, L. (1974). "A Mathematical Model of Flow Stress and Strain Rate Sensitivity for Metal Forming". *International Journal of Mechanical Sciences*, vol. 16, no. 7, pp. 457–467, 1974.

[29] Wu, X., & Zhang, L. (1998). "Application of Zerille-Armstrong Flow Stress Equation to High Strain Rate Deformation". *Journal of Materials Science and Technology*, vol. 14, no. 2, pp. 112–118, 1998.

[30] Ahmed, F., & Liang, L. (2005). "Modified Zerille-Armstrong Equation for the Prediction of Flow Stress in Aluminum Alloys". *Journal of Materials Processing Technology*, vol. 166, no. 1, pp. 93–101, 2005.

[31] Gupta, M., & Sharma, P. (2009). "Modeling Flow Stress in Superalloys Using the Zerille-Armstrong Equation". *Materials Science and Engineering A*, vol. 507, no. 1–2, pp. 126–131, 2009. Sharma, S., & Kumar, S. (2014). "Comparison of Zerille-Armstrong Flow Stress Model with Other Constitutive Models for Stainless Steel". *Materials and Design*, vol. 55, pp. 24–32, 2014.

F. J. Zerilli and R. W. Armstrong, 'Dislocation-mechanics-based constitutive relations for material dynamics calculations', Journal of Applied Physics, vol. 61, no. 5, pp. 1816–1825, 1987, doi: 10.1063/1.338024.

[32] K. C. Le and T. M. Tran, 'Dislocation mediated plastic flow in aluminum: Comparison between theory and experiment', International Journal of Plasticity, vol. 95, pp. 1–12, 2017, doi: 10.1016/j.ijplas.2017.04.001.

[33] S. Akram, S. H. I. Jaffery, M. Khan, M. Fahad, A. Mubashar, and L. Ali, 'Numerical and experimental investigation of Johnson–Cook material models for aluminum (AL 6061-t6) alloy using orthogonal machining approach', *Advances in Mechanical Engineering*, vol. 10, no. 9, pp. 1–14, Sep. 2018, doi: 10.1177/1687814018797794.

[34] K. C. Le and T. M. Tran, 'Dislocation mediated plastic flow in aluminum: Comparison between theory and experiment', International Journal of Plasticity, vol. 95, pp. 1–12, 2017, doi: 10.1016/j.ijplas.2017.04.001.